Peertechz

PHARMACY GROUP

INTERNATIONAL JOURNAL OF
Pharmaceutical Sciences and Developmental Research

ISSN: 2640-7760 DOI: https://dx.doi.org/10.17352/ijpsdr

Hossein Faghihian and Firoozeh Torki*

Department of Chemistry, Naghshejahan Higher Education Institute, Isfahan, Iran

Received: 23 September, 2019
Accepted: 30 December, 2019
Published: 31 December, 2019

***Corresponding author:** Firoozeh Torki, Department of Chemistry, Naghshejahan Higher Education Institute, Isfahan, Iran, E-mail: f.torki58@naghshejahan.ac.ir; f.torki58@yahoo.com

Keywords: Phenylephrine; Magnetic support; Polypyrrole; Visible light degradation

https://www.peertechz.com

Check for updates

Research Article

Visible light and UV-assisted photodegradation of phenylephrine by bulk NiO and NiO immobilized on magnetic polypyrrole support

Abstract

The nanophotocatalysts; NiO and NiO immobilized on the surface of magnetized polypyrrole (NiO-PPY-Fe_3O_4) were synthesized and used for photodegradation of phenylephrine. The synthesized photocatalysts were characterized by FTIR, TG, XRD, BET, VSM, TEM and SEM techniques. Diffuse reflectance spectroscopy was used to measure the band gap nergy of the synthesized photocatalyst. Photoluminescence analysis was employed to estimate the electron-hole recombination. The results indicated that immoblization of NiO on the surface of the polypyrrole support increased its photocatalytic activity. Under visible light, the degradation efficiency obtained by bulk NiO was 38% which was increased to 71% after immobilization on the catalyst support. The increase was attributed to the shift of band gap energy to higher wavelenght as indicated by DRS tests, and to the lowering of electron–hole recombination as revealed by PL analysis. The catalyst support improved the regeneration ability of the photocatalyst. After five regeneration cycles, 90% of NiO-PPY-Fe_3O_4 activity was remained while for bulk NiO, the value was about 15%. The paramagnetic nature of NiO-PPY-Fe_3O_4 photocalyst facilitated its separation from the degradation solution without tedious filteration or centrifugation steps. In low concentrations, H_2O_2 showed an enhancing effect on the degradation but the effect was reversed in higher concentrations.

Introduction

Many pharmaceutical compounds are considerred as environmental pollutants and their presence even at very low concentration (ng.L^{-1}) may adversely influence the biological system [1]. These compounds are frequently detected in wastewaters, surface and ground waters and even in the treated wastewaters because the waste treatment facilities are not equipped to remove them. As a result, many streams and rivers are exposed to entrance of pharmaceutical compounds from stimulants and antibiotics to analgesics and antihistamines compounds.

Phenylephrine hydrochloride (Figure 1S) used for nasal congestion is considered as one of the most important pharmaceutical pollutant [2]. Several methods have been used for elimination of the pollutants from aqueous solution including sono degradation [3], Fenton oxidation [4], nanofiltration [5], adsorption [6] and advance oxidation processes [7,8]. Advanced oxidation process have also been intensively used for effective degradation of many organic pollutants [9-13]. The essential requirement for the AOP process is an adequate heterogeneous photocatalyst, which is irradiated by UV, visible or sunlight radiations to produce electron-hole pairs (e^-/h^+). The electron-hole pairs subsequently generate highly active species such as OH radicals. The radicals then react with the pollutant molecules adsorbed on the surface of the photocatalyst [14,15].

The method is capable to destroy environmentally persistent pollutants by using photocatalysts activated by photons with energy higher or equal to the band gap energy of the photocatalyst. When the photon is absorbed by photocatalyst particle, an Electron (e^-) from the Valence Band (VB) is transferred to the Conduction Band (CB), generating a hole (h^+) in the VB. The e^- and h^+ can recombine on the surface or in the bulk of the particles releasing the energy as heat, or migrate to the photocatalyst surface where they can react with pollutant molecules absorbed on the surface of the particle. In the presence of water molecules, electrons are transferred from water molecule to the positive holes to produce $^{\circ}$OH radicals which are powerful oxidants and react with organic and toxic compounds. $^{\circ}$OH radicals play an important role in initiating oxidation reactions, especially for substances that are weakly absorbed on the photocatalyst surface.

Citation: Faghihian H, Torki F (2019) Visible light, and UV-assisted photodegradation of phenylephrine by bulk NiO, and NiO immobilized on magnetic polypyrrole support. Int J Pharm Sci Dev Res 5(1): 016-024. DOI: https://dx.doi.org/10.17352/ijpsdr.000023

The nano-sized photocatalyst possesses many advantages over their micro-sized counterparts, including higher degradation efficiency, proper mineralization potential, and higher efficiency with visible light. However, separation of the nano-sized photocatalysts from degradation solution is usually imperfect and time consuming. The nano-sized particles also tend to aggregate to large clusters, leading to lower specific surface area and lower degradation efficiency [16]. To eliminate these drawbacks, the particles can be magnetized by the aid of Fe_3O_4. The magnetized photocatalyst can be readily removed by use of a magnetic bar put outside of degradation vessel [17].

In photocatalytic degradation, recombination of electron/hole is a common problem, which adversely influence the efficiency of the photocatalyst. The process can be quenched or eliminated by immobilizing of the photocatalyst on the surface of an adequate support or an isolator. The conducting polymers such as polypyrrole (PPY) are potential candidates to reduce the aggregation of the nano-sized particles and to lower the electron-holes recombination.

This research was focused on the preparation of a magnetic polypyrrole composite (Fe_3O_4-PPY) to use it as the support for NiO photocatalyst. The synthesized photocatalyst and the bulk NiO were then used for degradation of phenylephrine under visible light, and UV irradiations.

Experimental

Materials and methods

All chemicals, including pyrrole (C_4H_5N), iron (III) chloride ($FeCl_3.6H_2O$), iron (II) chloride ($FeCl_2.4H_2O$), hydrochloric acid (HCl), sodium hydroxide (NaOH), m-cresole, amuminum persulphate (APS), $NiCl_2.6H_2O$, hydrogen peroxide (H_2O_2), were purchased from Merck company (Germany).

Characterization of the samples

Characterization of the synthesized photocatalyst was performed by different techniques including; FTIR, TG-DTG, XRD, SEM, BET (Brunauer–Emmett–Teller). The FTIR spectra were prepared on Nicolet single beam Impact 400D, Perkin Elmer Spectrophotometer (USA), in the region of 4000–400cm^{-1} by use of KBr pellet. An X-ray diffractometer (XRD JEOL100CX) was used to prepare the XRD patterns of the samples with CuK_α radiation (λ=1.788 A) operated at 40kV and 30mA. Field emission scanning electron microscopy (FESEM) images, and energy dispersive analysis of X-rays (EDAX) spectra were prepared by use of a JSM-6701F instrument (Japan). Thermal curves were prepared by a Perkin-Elmer thermal analyse; TG; model SSC-5200, (USA). Photoluminescence analysis (PL) was performed by a Cary Eclipse, FL0906M003 instrument (USA). Diffuse reflectance spectroscopy (DRS) by use of a UV-VIS model V-670 (Japan) was employed to study the band gap energy of the photocatalysts. Vibrating sample magnetometer (VSM, LDJ Electronics Inc Model 9600, Quantum Design USA) was used to measure the magnetization of the sample. Nitrogen adsorption-desorption isotherms were constructed by use of a BET (Brunauer Emmett Teller), Belsorp max instrument, BEL Company, (Japan). The concentration of phenylephrine (PHE) was measured by high performance liquid chromatography (HPLC), Aligent Technology 1200 series, (USA) by use of an ODS Hypersil C18, 250mm×4.7 mm, 5µ (Particle Size) column and a UV detector operated at 215nm. The degradation products were identified by a GC-MS instrument, 5975C Agilent, (USA) with a Bpx 30m×0.25mm×0.25µm capillary column.

Preparation of Fe3O4, Fe3O4-PPY composite

Synthesis of Fe_3O_4 nanoparticles and Fe_3O_4-PPY was performed by the method described by Torki, et al., [18]. Briefly, 10.8g of $FeCl_3.6H_2O$, and 3.98g of $FeCl_2.4H_2O$ were transferred into a beaker, under N_2 atmosphere, 50mL of HCl (0.5M) was added, and the mixture was shaken for proper homogenization. The pH of the solution was adjusted to 11 by drop wise addition of NaOH solution. The solid product was then separated by a magnet bar put outside of the vessel. It was thoroughly washed with distilled water until the filtrate become neutral. The product was dried at 60°C for 8h [19].

The magnetite composite Fe_3O_4-PPY was prepared by oxidative polymerization of pyrrole in the presence of APS solution [20]. 1.0 g of as-synthesized Fe_3O_4 nanoparticles was added into aqueous solution of APS (0.5g in 20mL of distilled water). The mixture was homogenized by sonication for 1h and then transferred into a 250mL two-neck flask. 0.5mL of pyrrole was added and the mixture was shaken at 25°C for 8h under N_2 atmosphere. The optimized amounts of materials were given in Table 1S. The black-coloured product (Fe_3O_4-PPY) was magnetically separated and thoroughly washed with deionized water and methanol and dried at 60°C for 24h (Figure 2Sa), [21].

Preparation of NiO and Fe3O4-PPY-NiO nanophotocatalysts

The NiO nanoparticles were first prepared as follows

12.0g of $NiCl_2.6H_2O$ was dissolved in 30mL of deionized water, the pH was adjust to 11.0 by addition of 0.1M NaOH solution. The precipitate; $Ni(OH)_2$ was separated by filtration, dried at 100°C and calcined at 550°C for 3h [22].

The Fe_3O_4-PPY-NiO nanophotocatalyst was prepared through the method described by Nalage [23], (Figure 2Sb). Concisely, 1.0g of Fe_3O_4@PPY and 1.0g of NiO nanoparticle were dispersed in 20mL of m-cresol solution and the mixture was refluxed for 15h at room temperature under N_2 atmosphere. The magnetized photocatalyst was collected by use of a magnet bar put outside of the vessel. It was thoroughly washed with deionized water and methanol and dried at 70°C for 6h. In the same manner, several photocatalysts with different NiO content (10%-80%) was prepared [23].

Photodegradation of the pollutant

The degradation experiments were carried out in a light tight reactor consisting of a cylindrical Pyrex-glass cell, a medium pressure Hg lamp (60W, Philips), and a fluorescent lamp (60W) located 10cm above the degradation cell. Known

Citation: Faghihian H, Torki F (2019) Visible light, and UV-assisted photodegradation of phenylephrine by bulk NiO, and NiO immobilized on magnetic polypyrrole support. Int J Pharm Sci Dev Res 5(1): 016-024. DOI: https://dx.doi.org/10.17352/ijpsdr.000023

amount of photocatalyst (0.2g) was added into 25mL of phenylephrine solution. The suspension was shaken for 30min at dark and then was irradiated for 240min. The photocatalyst was magnetically separated and the PHE concentration in the remaining solution was measured by HPLC-UV at λ 215 nm. The degradation efficiency was calculate by the following equation:

$$D\ (\%) = [(C_o - C)/C_o] \times 100 \quad (1)$$

Where C_o and C are respectively the PHE concentration before and after irradiation.

Results and Discussion

Characterization of the synthesized photocatalyst

In the SEM image of Fe_3O_4-PPY given in Figure 3Sa. The formation of uniform spherical-shaped particles were clearly observed. The particles were mostly aggregated forming clusters of the particles. After introduction of NiO, the molecules were homogeneously distributed on the surface of the magnetized composite and the morphology of the photocatalyst was remained unchanged. The average particles size of Fe_3O_4-PPY and Fe_3O_4-PPY-NiO was respectively 45 and 65nm. The increase in the particle size of Fe_3O_4-PPY-NiO was attributed to the coordination bond formed between the free electron pair of N atoms of PPY [23] and NiO molecule according to the scheme illustration given in Figure 3Sb.

In the XRD pattern the relative intensity and positions of the lines were in good agreement with the Fe_3O_4 reference (JCPDS #65-3107), (Figure 4Sa) and NiO reference (JCPDS# 47-1049) [24,25] (Figure 4Sb). The average particle sizes of Fe_3O_4 and NiO was calculated by Scherrer's equation:

$$D=0.94\lambda/SSCOS\theta \quad (2)$$

Where D is the average size and ß stands for the full-width at half-height of the peaks. The average particle size of Fe_3O_4 and NiO were respectively 14 and 25 nm.

The XRD pattern of Fe_3O_4-PPY-NiO sample, (Figure 4Sc) the presence of diffraction lines belonged to Fe_3O_4 structure was observed at 2θ of 41.5, 50.7, 63, 67, 74.5°, and those related to NiO were recorded at 2θ of 37, 43.5, 63 and 76°.

From the EDAX analysis of Fe_3O_4-PPY-NiO, the presence of Fe, O, Ni, C, N atoms on the surface of the photocatalyst was detected (Figure 5S). According to the map of elements represented in Figure 6S, it was concluded that the elements were uniformly distributed on the surface of the synthesized photocatalyst. The uniform distribution of NiO on the surface of the support is very advantageous for enhanced degradation efficiency.

The surface area of the samples measured by N_2 adsorption-desorption isotherms indicated that after immobilization of NiO on the surface of magnetized support, the surface area was reduced from 62.2 to 34.5m^2g^{-1} (Table 1). With lower surface area, it was expected to obtain lower degradation efficiency because lower amount of the pollutant was adsorbed on the photocatalyst surface, but immobilization of NiO on the surface of the magnetized support increased the efficiency of the photocatalysts by lowering the electron-hole recombination.

Table 1: Surface area of the samples.

No.	Sample	Surface area (m^2g^{-1})
1	NiO	53.2
2	Fe_3O_4-PPY	62.2
3	Fe_3O_4-PPY–NiO	34.5

In the FT-IR spectrum of Fe_3O_4 (Figure 7Sa), the adsorption band appeared at 470cm^{-1} was attributed to the characteristic Fe-O band and the peak at 1400cm^{-1} belonged to OH in-plane vibration of water molecules. The peaks appeared at 1600 and 3400cm^{-1} were related to water molecules adsorbed on the surface. The Fe-O band of Fe_3O_4-PPY, observed in Figures 7Sb,c slightly shifted to lower wave number. This reflects the effect of coordination interaction between Fe_3O_4 nanoparticle and polypyrrole chain [26]. In the spectra of Fe_3O_4-PPY (Figure 7Sb), and Fe_3O_4-PPY-NiO (Figure 7Sc), the characteristic absorption bands of polypyrrole were observed. The bands at 1080 and 900cm^{-1} were arisen respectively from CH in plane and CH out-of-plane vibration, indicating the successful polymerization of pyrrole [27]. The bands at 1500 and 1474cm^{-1} were respectively attributed to C–N and C–C asymmetric and symmetric ring stretching of PPY [26]. The peak at 1400cm^{-1} was attributed to the stretching band related to C=C of PPY ring. The weak bands of NH and CH stretching vibration of polypyrrole appeared respectively at 3404 and 2358cm^{-1} and the band at 3404cm^{-1} related to symmetrical stretch vibration of NH group has been buried under board OH peak of water molecules at 3400cm^{-1} [28] . From the results, it was concluded that the polymerization was successfully performed. In Fe_3O_4-PPY–NiO sample, the NiO stretching and vibrating band at 626cm^{-1} was observed. The main absorption band at 1600cm^{-1} belonged to water molecules became more intense due to the adsorption of water molecules by NiO nanoparticles. The absorption band at 3400cm^{-1} related to Fe_3O_4 was disappeared because of adsorption of water molecules by NiO particles.

In the thermal curves (TG-DTG) of Fe_3O_4-PPY-NiO represented in Figures 8Sa,b, a continuous weight loss peak from 25-800°C with two distinct steps was observed. The weight loss peak appeared between 80-15°C was attributed to the elimination of water molecules and unreacted monomer [23]. The second weight loss started from 500°C and ended at 800°C was attributed to the decomposition of PPY molecules. It was reported that pure PPY decomposed around 150°C, and after combination with nanoparticles, its thermal decomposition shifted to higher temperature (600-800°C) [29,30].

From the magnetization curves of Fe_3O_4, Fe_3O_4-PPY and Fe_3O_4-PPY-NiO given in Figures 1a-c, it was concluded that the samples were supper paramagnetic in nature and no hysteresis, neither coactivity was observed. The saturation magnetization of Fe_3O_4, Fe_3O_4-PPY and Fe_3O_4-PPY-NiO was respectively 80.2, 58.3, and 55.8$emug^{-1}$. The significant decrease on the saturation magnetization of Fe_3O_4-PPY-NiO was attributed to the presence of non-magnetic materials; PPY and NiO on the structure of the composite.

Citation: Faghihian H, Torki F (2019) Visible light, and UV-assisted photodegradation of phenylephrine by bulk NiO, and NiO immobilized on magnetic polypyrrole support. Int J Pharm Sci Dev Res 5(1): 016-024. DOI: https://dx.doi.org/10.17352/ijpsdr.000023

However, the magnetic property of the synthesized photocatalyst was sufficient for removal of the used photocatalyst by putting a magnet bar outside of the vessel. The magnetized particles were collected on the internal surface of the vessel within two second and immediately redistributed when the magnet bar was removed (Figure 1d).

Optical properties of the photocatalysts

The absorption edges of Fe_3O_4-PPY-NiO and NiO were obtained by DRS spectra (Figures 2a,b). The optical band gap (E_{gopt}) was obtained by equation 3.

$$E_{gopt}\ (ev) = h\upsilon = hc/e\lambda_{edge} \quad (3)$$

The constant parameter of hc/e are equal to 1240 and Eq.3 was simplified as Eq. 4

$$E_{gopt}\ (ev) = 1240/\lambda_{edge\ (nm)} \quad (4)$$

Where h is Planck's constant, c is the speed of light in the vacuum ($3\times10^8 m.s^{-1}$), e is the electron charge, λ (m) is the wavelength obtained from the intersection point of the horizontal and vertical parts of the absorption curve [31].

The absorption edge of NiO and Fe_3O_4-PPY-NiO were respectively at 364 and 406nm and the related band gap energy calculated by Eq. 4 was respectively 3.4 and 3.0 eV. The significant shift to lower energy, happened after immobilization of NiO on the magnetized support, was very beneficial for visible light-assisted degradation of the pollutant.

Similar observation was made by Singh who studied the degradation efficiency of TiO_2 immobilized on polyaniline catalyst support and reported higher degradation efficiency for brilliant blue [32].

The charge separation efficiency of the photocatalysts was determined by PL spectra. The samples were excited at 227 nm, and the emission peaks were recorded at 541 and 549 nm respectively for NiO and Fe_3O_4-PPY (Figures 3a,b). In Fe_3O_4-PPY-NiO sample (Figure 3c), the peaks at 541 belonged to

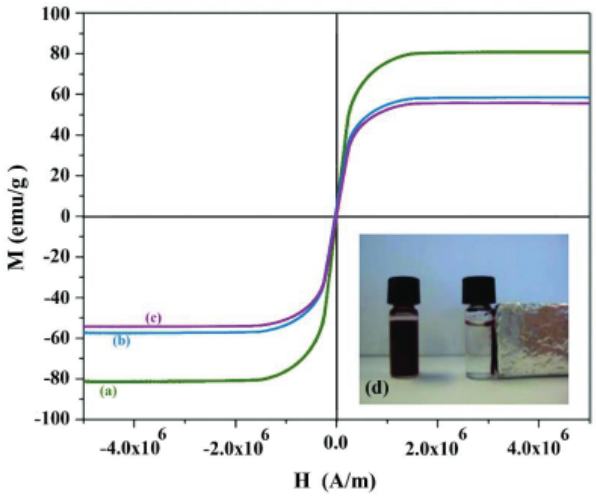

Figure 1: Magnetization curves of Fe_3O_4 (a), Fe_3O_4@PPY (b), Fe_3O_4@PPY-NiO (c).

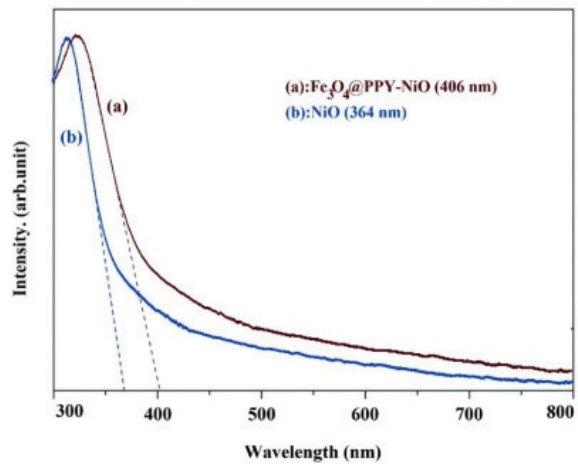

Figure 2: DRS curves of Fe_3O_4@PPY-NiO (a), NiO (b).

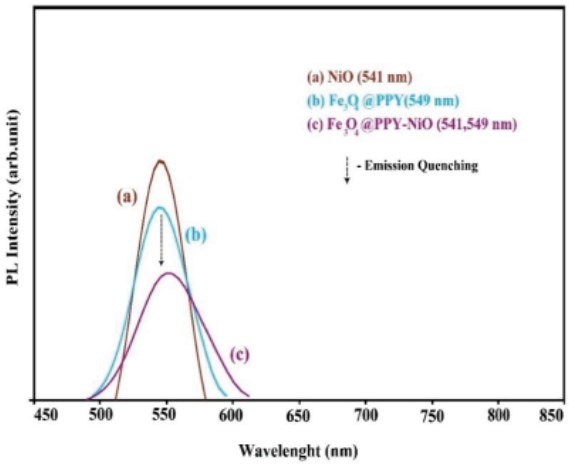

Figure 3: PL curves of NiO (a), Fe_3O_4@PPY-NiO (b), Fe_3O_4@PPY (c).

NiO and the peak at 549 were overlapped and appeared with lower intensities indicating that after immobilization of NiO on the PPY-Fe_3O_4 support because of lower electron-hole recombination, the activity of charge carriers was decreased and the photoluminescence emission was quenched.

Similar observation was made by Akhundi, who grafted Ag_2SO_4 onto g-C_3N_4 and Fe_3O_4/AgI/Ag_2CrO_4 and reported that the photoluminescence intensity of the sample was significantly quenched [33,34].

Photocatalyst performance

The initail degradtion experiment was performed by preparation of a suspension comprising of 25mL of PHE solution ($500mg.L^{-1}$) and 0.2g nanophotocatalys. The stock solution was prepared by dissolving of 200mg of PHE in 100mL of deionized water. The calibration curve was plotted over the concentration range of $10-700mgL^{-1}$. The suspention was shaken for 30min at dark untill adsorption/desorption process was at equilibration. After equilibration, the degradtion solution was irradiated for predeterminted time, the photocatalyst was removed and the PHE concentration was measured in the remaining solution by HPLC-UV at 217nm. The mobile phase was a mixture of KH_2PO_4

Citation: Faghihian H, Torki F (2019) Visible light, and UV-assisted photodegradation of phenylephrine by bulk NiO, and NiO immobilized on magnetic polypyrrole support. Int J Pharm Sci Dev Res 5(1): 016-024. DOI: https://dx.doi.org/10.17352/ijpsdr.000023

buffer (pH 4.7) and methanol (70:40 v/v). The flow rate was adjusted at 1.0mLmin^{-1}. The retention time for PHE was found to be at 2.5 min [2]. From the chromatograms of the samples taken before and after degradation it was concluded that the intensity of PHE peak (RT 2.5min) was significantly decreased after degradation indicating the good performance of the photocatalyst for degradation of the pollutant (Figures 9Sa,b).

The statistical data of the method is given in Table 2S. the R^2 value of 0.9972 for calibration curve, and the acceptable RSD value indicated the the applicability of the method.

To optimize the degradation efficiency, the effect of different influencing parameters on the degradation efficiency were studied.

Optimizing of degradation efficiency

Effect of initial PHE concentration: The effect of initial PHE concentration was evaluated in the concentration range of 20-1000 mgL^{-1} (Figure 4). At low concentration (20-50mgL^{-1}), the degradation efficiency under visible light was 85 and 60% respectively with NiO-PPY-Fe_3O_4 (S2) and NiO (S4). Evan at concentration of 1000mgL^{-1}, 70% of the pollutant molecules were degraded by NiO-PPY-Fe_3O_4. This showed the high performance of the synthesized catalyst for degradation of the pollutant under visible light. The higher efficiency obtained at low concentration was attributed to the fact that the pollutant molecules were properly adsorbed on surface of the catalyst where the generated OH radicals easily reacted with them. This is very advantageous for elimination of the pollutant from the waste streams in which the pollutant concentration is usually low. However the degradation of the pollutant by UV irradiation was always higher than visible light because lower fractions of the visible light had sufficient energy to excite the photocatalyst molecules.

The degradation efficiency obtained by Fe_3O_4-PPY-NiO was much higher than the value obtained by bulk NiO. This was attributed to the enhancing effect of catalyst support through lowering the band gap energy of the photocatalyst and limiting the electron-hole recombination as discussed in section 3.2.

Effect of photocatalyst dosage: Degradation of PHE was studied with different photocatalysts dosage (0.001-0.35g) added to 25mL of the pollutant solution (500mgL^{-1}). By increasing of catalyst dose, more adsorption sites were supplied for the pollutant, more photocatalyst molecules (NiO) was provided, therefore, the degradation was increased through effective interaction between OH radicals and the pollutant molecules. With catalyst dose beyond 0.2g, the degradation first became constant and then was slightly decreased owing to the aggregation of the photocatalyst nanoparticles which decreased the surface area of the photocatalyst. With lower surface area lower amount of the pollutant are adsorbed and the photocatalyst molecules are not fully accessible [35]. (Figure 10S). With the same amount of the photocatalyst, the degradation efficiency obtained by Fe_3O_4-PPY-NiO was higher than that of bulk NiO. This indicated the enhancing effect of catalyst support on the efficiency of the photocatalyst.

Effect of irradiation time: The degradation efficiency was evaluated for irradiation time of 0 to 240min (Figure 5). By increasing of irradiation time, the degradation was initially increased until the equilibration was established within 240min.

With the increasing of irradiation time, more OH$^{\circ}$ radicals were generated and at equilibrium, the generated OH radicals and pollutant molecules adsorbed on the surface of the photocatalyst were at steady state. The degradation efficiency obtained by Fe_3O_4-PPY was insignificant throughout the studied time. The activity of Fe_3O_4-PPY-NiO was higher than bulk NiO at each interval time. The degradation efficiency obtained by Fe_3O_4-PPY-NiO under UV and visible light irradiations became closer (respectively 81% and 71%). This was highly beneficial for degradation of the pollutant by visible light energy.

Effect of pH: The pH of the degradation solution has important influences on the degradation efficiency through changing the amount of adsorbed pollutant on the surface of photocatalyst and the quantity of the generated hydroxyl radicals ([36]. In this work, the effect of pH on the degradation efficiency was studied on pH range of 3-9 (Figure 6). The maximal degradation was obtained at pH 7. To evaluate the effect of pH on the surface charge of the photocatalyst, its pH_{pzc} was determined. As indicated in (Figure 6), the PH_{pzc} of the photocatalysts was at pH 7. At this pH, the surface of the

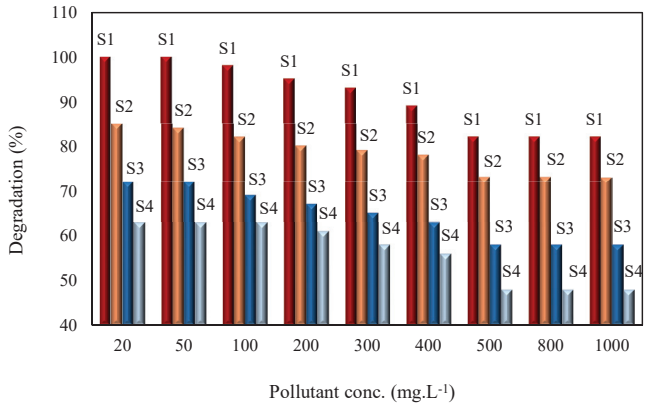

Figure 4: Effect of the initial concentration of PHE.

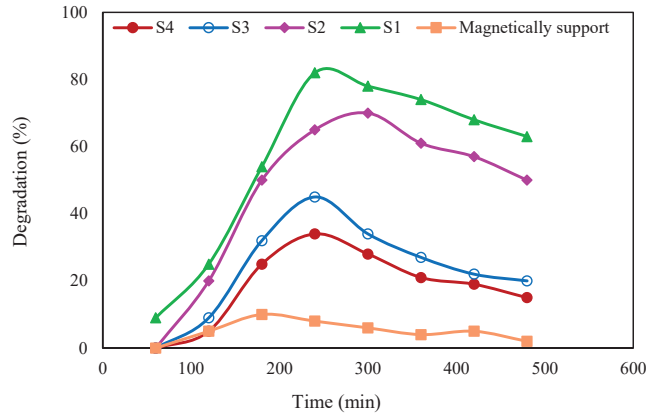

Figure 5: Effect of iraddiation time on PHE degradation.

Citation: Faghihian H, Torki F (2019) Visible light, and UV-assisted photodegradation of phenylephrine by bulk NiO, and NiO immobilized on magnetic polypyrrole support. Int J Pharm Sci Dev Res 5(1): 016-024. DOI: https://dx.doi.org/10.17352/ijpsdr.000023

photocatalysts was neutral and the pollutant molecules were absorbed on the surface of photocatalyst by wan der walls attraction forces [37]. In acidic solutions, functional groups of PHE and PPY molecules were protonated and their charge was converted to positive. Therefore, the repulsion force between the PHE molecules and the catalyst surface limited the adsorption of the pollutant.

In acidic solutions, functional groups of PHE and PPY molecules were protonated and their charge was converted to positive. Therefore, the repulsion force between the PHE molecules and the catalyst surface limited the adsorption of the pollutant. At pHs higher than pH_{pzc}, the surface of the catalyst was negatively charged, the PHE molecules were deprotonated and their charge became negative. Hence the repulsion force again reduced the number of adsorbed pollutant molecules. Moreover, at alkaline pHs, according to the following reactions, the OH° radicals were converted to new radicals with less active species [38].

$$OH^\circ + HO_2^- \rightarrow H_2O + O_2^\circ \quad (5)$$

$$OH^\circ + H_2O_2 \rightarrow H_2O + O_2H^\circ \quad (6)$$

Effect of NiO content: To study the effect of NiO content of the photocatalyst on the degradation efficiency, the degradation experiments were conducted in the presence of photocatalysts with different NiO content (10%-80%) (Figure 7). With the catalysts containing low content of NiO, limited extent of degradation was obtained owing to the limited number of the generated OH radicals. With increasing of NiO content, the degradation efficiency was increased and the optimized efficiency was obtained with the photocatalyst containing 50% of NiO. When the NiO content exceeded to 50%, aggregation of the particle reduced the surface area of the photocatalyst resulting lower degradation efficiency.

Similar results were reported by Pourtaheri, who prepared a photocatalyst by immobilization of NiO on the surface of clinoptilolite and reported that the maximal efficiency of (80%) was obtained with the catalyst containing 13% of NiO [39].

The effect of temperature on the degradation efficiency: In this work, the degradation efficiency was measured at different temperatures of 25, 35, 45 and 55°C (Figure 8). The

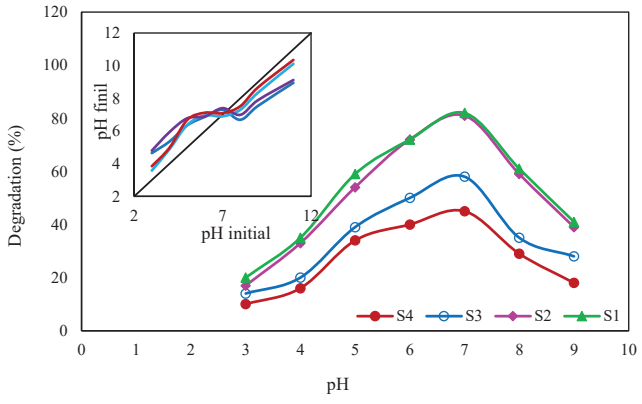

Figure 6: Effect of pH on PHE degradation.

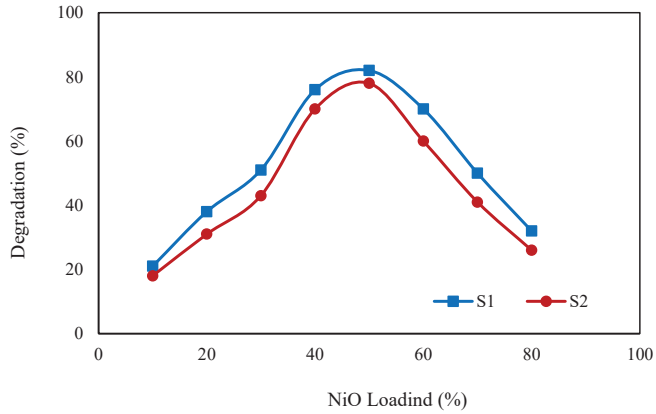

Figure 7: Effect of NiO loading on PHE degredation.

results indicated that at higher temperature, lower degradation efficiency was obtained. It was suggested that by increasing of temperature, the amount of dissolved oxygen was decreased.

The dissolved oxygen increased the generation of hydroxyl radical through Eqs. 7-10. By capturing the photo-induced electrons, $O_2^{\circ-}$ radicals were produced (Eq. 7) which then reacted with h^+ generating H_2O_2 (Eqs. 8-9). H_2O_2 was finally converted to OH^- radicals (Eq. 10).

$$O_2 + e^- \rightarrow O_2^{\circ-} \quad (7)$$

$$O_2^{\circ-} + h^+ \rightarrow H_2O_2 + O_2 \quad (8)$$

$$O_2^{\circ-} + e^- \rightarrow H_2O_2 + H^+ \quad (9)$$

$$H_2O_2 + e^- \rightarrow OH^- + OH^\circ \quad (10)$$

Similar observation was reported by Shivaraju, who studied the effect of temperature on the photocatalytic degradation efficiency organic matters [40].

Addition of H_2O_2

The effect of H_2O_2 on the degradation efficiency was studied by addition of H_2O_2 solution into 25mL of degradation solution ($500mgL^{-1}$) (Figure 9). It was concluded that by increasing of H_2O_2 concentration, the degradation efficiency was firstly increased owing to the generation of extra OH radicals through reactions 11-12 and the maximized efficiency was obtained with 0.1M. H_2O_2 concentration.

However, by exceeding the optimum concentration, the degradation efficiency was declined because at higher concentration, H_2O_2 scavenged the hydroxyl radicals through Eqs.13 and 14. The excess H_2O_2 reacts with OH° radicals to form weaker HO_2° radicals [41].

$$H_2O_2 + e^- \rightarrow OH^\circ + OH^- \quad (11)$$

$$H_2O_2 + O_2^\circ \rightarrow OH^\circ + OH^- + O_2 \quad (12)$$

$$H_2O_2 + OH^\circ \rightarrow H_2O + OH_2^\circ \quad (13)$$

$$HO_2^\circ + OH^\circ \rightarrow H_2O + O_2 \quad (14)$$

Tseng, et al., studied the effect of hydrogen peroxide on the photocatalytic degradation of monochlorobenzene in the presence of TiO_2 and reported that degradation efficiency in the presence of hydrogen peroxide was enhanced [41]. Barba

Citation: Faghihian H, Torki F (2019) Visible light, and UV-assisted photodegradation of phenylephrine by bulk NiO, and NiO immobilized on magnetic polypyrrole support. Int J Pharm Sci Dev Res 5(1): 016-024. DOI: https://dx.doi.org/10.17352/ijpsdr.000023

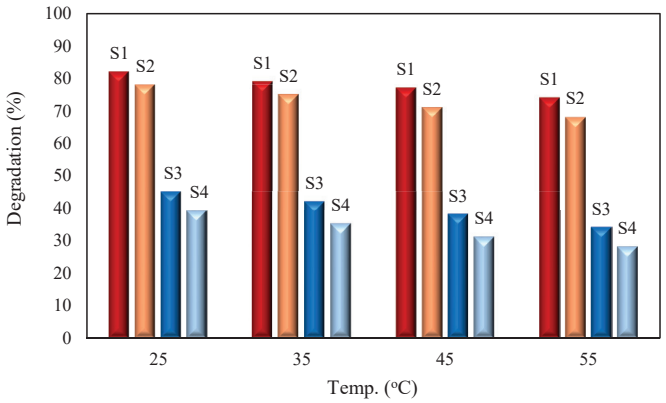

Figure 8: Effect of dissolved oxygene on PHE degradation.

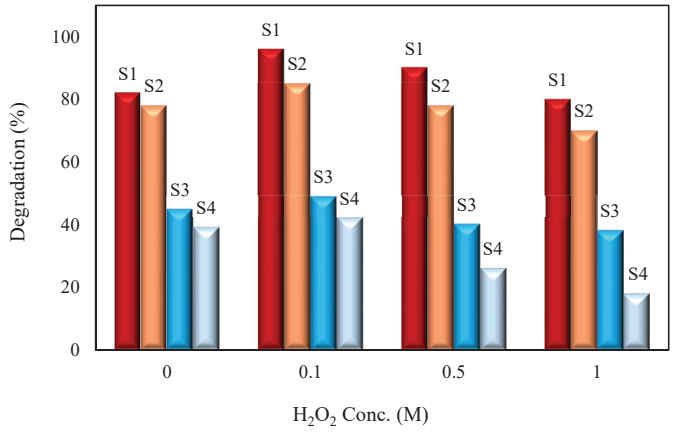

Figure 9: Effect of dissolved oxygene on PHE degradation.

who studied the photodegradation of some drugs reported that addition of H_2O_2 increased the of degradation efficiency [42,43].

Regeneration of the photocatalyst

One of the most important advantages of magnetized photocatalyst is the ease of separation of catalysts from the reaction solution which facilities the regeneration of the photocatalyst. In this work, the used photocatalyst was separated from the solution by a magnet bar put outside of the degradation cell. The photocatalyst was then regenerated by heat treatment at 250°C for 6h to eliminate the degradation products deposited on the surface of the photocatalyst. The regenerated photocatalyst was reused for degradation of PHE at optimized conditions. The process was repeated for five successive regeneration steps (Figure 11S). It was concluded that the activity of the catalysts, in terms of the PHE degradation efficiency was slowly decreased in each cycle, and the decrease was more pronounced with increasing the number of reusing cycles.

However, after fifth regeneration cycle, 80% of the initial efficiency was observed for S1 sample. The decrease was explained by partial occupation of adsorption sites by degradation products, or dislocation and aggregation of NiO particles during heat treatment.

GC-MS Analysis and identification of degradaton products

The degradation products of PHE were analyzed by full scan mode of GC-MS. Aliquots of PHE solutions after degradation and a sample containing standard PHE were prepared. The extration of degradation products from aqueous solution was done by chloroform. It note that PHE is unsoluble in chlorofom but degradation products extracted. The Mass spectrum of PHE was similar to that of reference sample (Figure 12S). The GC spectra of PHE before and after degradation is displyed in Figure 13S. To identify the degradation fagments, they were separated from the solution by extraction with chloroform. and the mass spectra of the identified degradation products is represented in Figure 14S.

The MS spectrum of degradation products were concluded that the peaks appeared at retention time of 3.8, 3.9, 4.7, 4.8, 7.7 and 7.5mins beonged to the degradation products and the peak appeared at RT 11.0 was related to the remaining PHE. The identified compounds are listed in Table 3S. The main degradation products are di-sec-buthyl ether, di-sec-buthyl acetal, benzyl ether, 4- oxo-pentanoic acid and 4-chlorobenzaldehyde.

The aim of AOPs process is to mineralize the organic pollutant and to convert them into H_2O and CO_2. To evalute the mineralization degree of the pollutant, the Total Organic Carbon (TOC) of the degradtion solution was measured before and after irradiations. It was concluded that 85% of degraded polutant was mineralized. Therefore, the concentration of the identified degradtion products was very small.

Conclusions

In this work, a magnetized support was prepared by in-situ oxidative polymerization of polypyrrole in the presence of Fe_3O_4. The support was then employed as the catalyst support for NiO photocatalyst. The synthesized catalyst was characterized by different techniques. The SEM images showed that the particle size of Fe_3O_4-PPY and Fe_3O_4-PPY-NiO were respectively 45 and 65nm. The DRS analysis indicated that band gap energy of NiO after immobilization on thes surface of the support shifted to lower energy which was benficial for visible light degradation of the pollutant. PL analysis of the photocatalysts showed that after embeding of NiO on the suport, the electron-hole recmbination was significantly quenched leading to higher degradtion efiiciency. The synthesized photocatalyst, and the bulk NiO, were used for degradtion of PHE under UV and visible light irradiaions. The degradation process was kinetically fast and the equilibrium was achieved within 4h of irradiaton. The used magnetized nanophotocatalyst was removed from the degradation solution by applying external magnetic field and was regenerated by heat treatment at 250°C. Most of its initial activity was remained after five regeneration cycles.

Acknowledgment

The authors of this paper wish to appreciate the co-operation of the Islamic Azad University, Shahreza Branch

Supplementry Figures & Tables

Citation: Faghihian H, Torki F (2019) Visible light, and UV-assisted photodegradation of phenylephrine by bulk NiO, and NiO immobilized on magnetic polypyrrole support. Int J Pharm Sci Dev Res 5(1): 016-024. DOI: https://dx.doi.org/10.17352/ijpsdr.000023

References

1. Trawinski J, Skibinski R (2017) Studies on photodegradation process of psychotropic drugs, a review. Environ Sci Pollut Res 24: 1152–1199. Link: http://bit.ly/2QJNnt9

2. Patel H, Chauhan P, Prajapati BD, Shah SK (2014) RP-HPLC methods development and validation for simultaneous estimation for tropic amid and phenylephrine hydrochloride in ophthalmic formulation. Int J Institu Pharm Life Sci 4: 2249-6807.

3. Agnieszka M, Juan CC, Olga C, Dariusz L, Kamil S (2016) Sonication and light irradiation as green energy sources simultaneously implemented in the synthesis of Pd-Fe- and Pt-Fe- doped TiO_2-based photocatalysts. J Mol Catal A- Chem 425: 1-9. Link: http://bit.ly/37tO68I

4. Soltani T, Lee BK (2016) Improving heterogeneous photo-Fenton catalytic degradation of toluene under visible light irradiation through Ba-doping in BiFeO3 nanoparticles. J Mol Catal A- Chem 425: 199-207. Link: http://bit.ly/39Ce8s7

5. Wang KY, Chung TS (2005) Characterization of flat composite nanofiltration membranes and their applications in the separation of Cephalexin. J Membrane Sci 247: 37. Link: http://bit.ly/37uJ6AB

6. Beltran NFA, Marce RM, Gormack PAG, Borrull F (2009) Molecularly imprinted solid phase extraction of cephalexin from waste water based matrices. J Sep Sci 32: 3319-3326. Link: http://bit.ly/2ZNPBMA

7. Namasivayam C, Kavith D (2002) Removal of Congo Red from water by adsorption onto activated carbon prepared from coir pith, an agricultural solid waste. Dyes Pigments 54: 47-58. Link: http://bit.ly/39BVMYw

8. Akhundi A, Habibi-Yangjeh A (2016) Facile preparation of novel quaternary g-C_3N_4/Fe_3O_4/AgI/Bi_2S_3 nanocomposites: magnetically separable visible-light-driven photocatalysts with significantly enhanced activity. RSC Adv 6: 106572-106583. Link: http://bit.ly/2MOSnf0

9. Sixto M, Julian B, Alfonso V, Christoph R (2001) Photocatalysis with solar energy at a pilot-plant scale: an overview. Appl Catal B Environ 35: 117. Link: http://bit.ly/37yMwlQ

10. Zhao X, Qu J, Liu H, Qiang Z, Liu R, et al. (2009) Photoelectrochemical degradation of anti-inflammatory pharmaceuticals at Bi_2MoO_6–boron-doped diamond hybrid electrode under visible light irradiation. Appl Catal B-Environ 91: 539–545. Link: http://bit.ly/2QI9Ir3

11. Elmorsi TM, Riyad YM, Mohamed ZH, Abd El Bary HM (2010) Decolorization of Mordant red 73 azo dye in water using H_2O_2/UV and photo-Fenton treatment. J Hazard Mater 174: 352-359. Link: http://bit.ly/2SNxFjv

12. Arany E, Szabo RK, Apatia L, Alapi T, Ilisz I, et al. (2013) Degradation of naproxen by UV, VUV photolysis and their combination. J Hazard Mater 262: 151-157. Link: http://bit.ly/35f6ErO

13. Eslami A, Amini MM, Yazdanbakhsh AR, Mohseni-Bandpei A, Safarid AA, et al. (2016) N,S co-doped TiO_2 nanoparticles and nanosheets in simulated solar light for photocatalytic degradation of non-steroidal anti-inflammatory drugs in water: a comparative study. J Chem Technol Biotechnol 91: 2693-2699. Link: http://bit.ly/2QkSfGi

14. Liu X, Iang CL, Wang H, Yang X, Lu L, et al. (2002) Usage of ultrafine anatase/TiO_2·nH_2O powder, photocatalysis and microstructure control for nano-crystalline TiO_2. Mater Sci Eng A 326: 235–239. Link: http://bit.ly/2QjhcBQ

15. Hsiao KC, Lia SC, Chen YJ (2007) Synthesis, Characterization and photocatalytic property of nanostructured Al-doped ZnO powders prepared by spray pyrolysis. Mater Sci Eng A 447: 71–76. Link: http://bit.ly/2ttLMQd

16. Francesco P, Letizia P, Fabrizio S, Claudio M, Erik O, et al. (2017) Influence of agglomeration and aggregation on the photocatalytic activity of TiO_2 nanoparticles. Appl Catal B: Environ 216: 80–87. Link: http://bit.ly/37wX1Go

17. Anna ZJ, Zuzanna B, Izabela W, Judyta S, Marcin J, et al. (2017) Magnetic semiconductor photocatalysts for the degradation of recalcitrant chemicals from flow back water. J Environ Management 195: 157-165. Link: http://bit.ly/2QhrfaC

18. Torki F, Faghihian H (2017) Sunlight-assisted decomposition of cephalexin by novel synthesized NiS-PPY-Fe_3O_4 nanophotocatalyst. J Photochem Photobiol A Chem 338: 49-59. Link: http://bit.ly/39ECQbJ

19. Wang J, Zheng S, Shao Y, Liu J, Xu Z, et al. (2010) Amino-functionalized Fe_3O_4@SiO_2 core-shell magnetic nanomaterial as a novel adsorbent for aqueous heavy metals removal. J Colloid Interf Sci 349: 293-299. Link: http://bit.ly/35hpOxm

20. Torki F, Faghihian H (2017) Photocatalytic activity of NiS, NiO and coupled NiS–NiO for degradation of pharmaceutical pollutant cephalexin under visible light. RSC Adv 7: 54651-54661. Link: https://rsc.li/36lr5om

21. Ramesan MT (2015) Preparation and properties of Fe_3O_4@PPY/polypyrrole/poly (pyrrole-co-acrylamide) nanocomposites. Int J Polym Mater Polym Biomat 62: 277-283. Link: http://bit.ly/35lyUcq

22. Zhao G, Mo Z, Zhang P, Wang B, Zhu X, et al. (2015) Synthesis of graphene/Fe_3O_4/NiO magnetic nanocomposites and its application in photocatalytic degradation the organic pollutants in wastewater. J Porous Mater 22: 1245–1253. Link: http://bit.ly/35gkb2h

23. Nalage SR, Navale ST, Patil VB (2013) Polypyrrole-NiO hybrid nanocomposite, Structural, morphological, optical and electrical transport studies. Measurement 46: 3268-3275. Link: http://bit.ly/39Da62L

24. Qiao M, Lei X, Ma Y, Tian L, Su K, et al. (2016) Well-defined core/shell Fe_3O_4@polypyrrole composite microspheres with tunable shell thickness, synthesis and their superior microwave absorption performance in the Ku band. Ind Eng Chem Res 55: 62-63. Link: http://bit.ly/35iwCL1

25. Sun X, Liu Y, Gao H, Gao PX, Lei Y (2014) Bimodular high temperature planar oxygen gas sensor. Front Chem 2: 57. Link: http://bit.ly/2FiswYU

26. Lamprakopoulos S, Yfantis D, Yfantis A, Schmeisser D, Anastassopoulou J, et al. (2004) An FT-IR study of the role of H_2O and D_2O in the aging mechanism of conductive polypyrrole. Synth Met 14: 229-234. Link: http://bit.ly/37qAmvo

27. Turcu R, Pana O, Nan A, Craciunescu I, Chauvet O, et al. (2008) Polypyrrole coated magnetite nanoparticles from water-based nanofluids. J Phys D: Appl Phys 41. Link: http://bit.ly/2ucptyZ

28. Zhao SY, Lee DK, Kim CW, Cha HG, Kim YH, et al. (2006) Synthesis of Magnetic Nanoparticles of Fe_3O_4@PPY and $CoFe_2O_4$ and Their Surface Modification by Surfactant Adsorption. Bull Korean Chem Soc 27: 237-242. Link: http://bit.ly/39u8YP7

29. Guo Z, Shin K, Karki AB, Young DP, Kaner RB, et al. (2009) Fabrication and characterization of iron oxide nanoparticles filled polypyrrole nanocomposites. J Nanopart Res 11: 1441–1452. Link: http://bit.ly/2MQ3PqQ

30. Marimuthu T, Mohamad S, Alias Y (2015) Needle-like polypyrrole-NiO composite for non-enzymatic detection of glucose. Synthetic Met 207: 35-41. Link: http://bit.ly/2QGrgDZ

31. Guo J, Guo J, Gu H, Wei H, Zhang Q, et al. (2013) Magnetite-polypyrrole metacomposites, dielectric properties and magneto resistance behavior. J Phys Chem C 117: 10191–10202. Link: http://bit.ly/2syETNP

32. Singh S, Mahalingam H, Singh PK (2013) Polymer-supported titanium dioxide photocatalysts for environmental remediation: a review. Appl Catal A general 462–463:178–195. Link: http://bit.ly/2u6NyHp

33. Akhundi A, Habibi-Yangjeh A (2016) Novel g-C_3N_4/Ag_2SO_4 nanocomposites, fast microwave-assisted preparation and enhanced photocatalytic performance towards degradation of organic pollutants under visible light. J Colloid Interf Sci 482: 165–174. Link: http://bit.ly/2QFniLT

Citation: Faghihian H, Torki F (2019) Visible light, and UV-assisted photodegradation of phenylephrine by bulk NiO, and NiO immobilized on magnetic polypyrrole support. Int J Pharm Sci Dev Res 5(1): 016-024. DOI: https://dx.doi.org/10.17352/ijpsdr.000023

34. Akhundi A, Habibi-Yangjeh A (2016) Codeposition of AgI and Ag_2CrO_4 on g-C_3N_4/Fe_3O_4 nanocomposite, novel magnetically separable visible-light-driven photocatalysts with enhanced activity. Adv Powder Technol 27: 2496-2506. Link: http://bit.ly/2QhrJgW

35. Pehlivan E, Altun T, Parlayici S (2008) Utilization of barley straws as biosorbents for Cu^{2+} and Pb^{2+} ions. J Hazard Mater 164: 982-986. Link: http://bit.ly/37tUoFp

36. Falahian Z, Torki F, Faghihian H (2018) Synthesis and Application of Polypyrrole/Fe_3O_4 Nanosize Magnetic Adsorbent for Efficient Separation of Hg^{2+} from Aqueous Solution. Global Challenges 2: 1700078-1700086. Link: Link: http://bit.ly/2SMkGP6

37. Suponik T, Winiarski A, Szade J (2015) Processes of Removing Zinc from Water using Zero-Valent Iron. Water Air Soil Pollut 226: 360. Link: http://bit.ly/35puykF

38. Spuhler D, Rengifo-Herrera JA, Pulgarin C (2010) The effect of Fe^{2+}, Fe^{3+}, H_2O_2 and the photo-Fenton reagent at near neutral pH on the solar disinfection (SODIS) at low temperatures of water containing Escherichia Coli k12. Appl Catal B Environ 96: 126–141. Link: http://bit.ly/37tPPLe

39. Pourtaheri A, Ejhieh AN (2015) Photocatalytic properties of incorporated NiO onto clinoptilolite nano-particles in the photodegradation process of aqueous solution of cefixim pharmaceutical capsule. Chem Eng Res Design 104: 835-834. Link: http://bit.ly/2ZMJ44t

40. Shivaraju HP (2011) Removal of Organic Pollutants in the Municipal Sewage Water by TiO_2 based Heterogeneous Photocatalysis. Int J Environ Sci 1: 1-10. Link: http://bit.ly/2trjgPc

41. Tseng DH, Juang LC, Huang HH (2012) Effect of oxygen and hydrogen peroxide on the photocatalytic degradation of monochlorobenzene in TiO_2 aqueous suspension. Int J photoenergy 5: 1-9. Link: http://bit.ly/2QKAKOR

42. Marin A, Barbas C (2004) LC/MS for the degradation profiling of cough-cold products under forced conditions. J Pharmaceut Biomed 35: 1035. Link: http://bit.ly/2QFx40G

43. Homayoon F, Faghihian H, Torki F (2017) Application of a novel magnetic carbon nanotube adsorbent for removal of mercury from aqueous solutions. Environ Sci Pollut Res 24: 11764-11778. Link: http://bit.ly/35j4Td6

Citation: Faghihian H, Torki F (2019) Visible light, and UV-assisted photodegradation of phenylephrine by bulk NiO, and NiO immobilized on magnetic polypyrrole support. Int J Pharm Sci Dev Res 5(1): 016-024. DOI: https://dx.doi.org/10.17352/ijpsdr.000023